Heavy-elements heritage of the falling sky

Alejandra Recio-Blanco, Emma Fernández-Alvar, Patrick de Laverny, Teresa Antoja, Amina Helmi, Aurélien Crida

A&A 648, A108 (2021)
https://doi.org/10.1051/0004-6361/202038943

Astronomy & Astrophysics

Heavy-elements heritage of the falling sky*

Alejandra Recio-Blanco[1], Emma Fernández-Alvar[1], Patrick de Laverny[1], Teresa Antoja[2], Amina Helmi[3], and Aurélien Crida[1]

[1] Université Côte d'Azur, Observatoire de la Côte d'Azur, CNRS, Laboratoire Lagrange, Nice, France
e-mail: arecio@oca.eu
[2] Institut de Ciències del Cosmos, Universitat de Barcelona (IEEC-UB), Barcelona, Spain
[3] Kapteyn Astronomical Institute, University of Groningen, Landleven 12, 9747, AD Groningen, The Netherlands

Received 16 July 2020 / Accepted 2 November 2020

ABSTRACT

Context. A fundamental element of galaxy formation is the accretion of mass through mergers of satellites or gas. Recent dynamical analyses based on *Gaia* data have revealed major accretion events in the history of the Milky Way. Nevertheless, our understanding of the primordial Galaxy is hindered because the bona fide identification of the most metal-poor and correspondingly oldest accreted stars remains challenging.
Aims. Galactic archaeology needs a new accretion diagnostic to understand primordial stellar populations. Contrary to α-elements, neutron-capture elements present unexplained large abundance spreads for low-metallicity stars, which could result from a mixture of formation sites.
Methods. We analysed the abundances of yttrium, europium, magnesium, and iron in Milky Way satellite galaxies, field halo stars, and globular clusters. The chemical information was complemented by orbital parameters based on *Gaia* data. In particular, we considered the average inclination of the orbits.
Results. The [Y/Eu] abundance behaviour with respect to the [Mg/Fe] turnovers for satellite galaxies of various masses reveals that higher-luminosity systems, for which the [Mg/Fe] abundance declines at higher metallicities, present enhanced [Y/Eu] abundances, particularly in the [Fe/H] regime between −2.25 dex and −1.25 dex. In addition, the analysis has uncovered a chemo-dynamical correlation for both globular clusters and field stars of the Galactic halo, accounting for about half of the [Y/Eu] abundance spread. In particular, [Y/Eu] under-abundances typical of protracted chemical evolutions are preferentially observed in polar-like orbits, pointing to a possible anisotropy in the accretion processes.
Conclusions. Our results strongly suggest that the observed [Y/Eu] abundance spread in the Milky Way halo could result from a mixture of systems with different masses. They also highlight that both nature and nurture are relevant to the formation of the Milky Way since its primordial epochs, thereby opening new pathways for chemical diagnostics of the build-up of our Galaxy.

Key words. Galaxy: abundances – Galaxy: halo – Galaxy: stellar content – Galaxy: formation

1. Introduction

The most primitive Galactic stars are essential to understand the formation of the Milky Way. Nevertheless, the robust identification of accreted objects is particularly challenging for stars with primordial abundances having at most 30 times less metals than the Sun ([Fe/H] $\lesssim -1.5$). Through clustering in only these parameter spaces (see for instance Belokurov et al. 2020), kinematical or dynamical indications of accretion can be misinterpreted as a result of parameter degeneracies (Jean-Baptiste et al. 2017; Di Matteo et al. 2019; Koppelman et al. 2020; Ratcliffe et al. 2020). Those indications need to be complemented by chemical diagnostics (Freeman & Bland-Hawthorn 2002), as the chemical evolution of a system strongly depends on its mass. Compared to the massive Milky Way, satellite galaxies generally present signs of protracted evolutions. This is because satellite galaxies are more metal deficient and show a variety of chemical patterns that should be possible to retrieve in the accreted populations that are now mixed with in situ formed stars.

The most commonly used chemical diagnostic of accretion is the α-elements (O, Mg, Si, S, Ca, Ti) ratio with respect to iron ([α/Fe]). Initially enhanced, the [α/Fe] abundance starts to strongly decline with metallicity after the supernovae Ia explosion rate reaches a maximum, dominating iron nucleosynthesis (Tinsley 1979; Matteucci & Greggio 1986). This produces a knee in the [α/Fe] versus [Fe/H] trend whose location provides constraints on the total mass of the system: the less massive the system, the more metal-poor is the [α/Fe] turnover (although see also other factors discussed in Suda et al. 2017). Unfortunately, this accretion diagnostic is not discriminating enough for stars in the Galactic halo, which have metallicities lower than the [α/Fe] turnover of most satellite galaxies. As a consequence, metal-poor field stars kinematically proposed to be members of ancient accreted satellites, such as the *Gaia*-Enceladus/Sausage (Helmi et al. 2018; Belokurov et al. 2018), have similar [α/Fe] abundances as non-members for [Fe/H] $\lesssim -1.5$ dex. These field stars only appear as a separate sequence at higher metallicity (Nissen & Schuster 2010; Fishlock et al. 2017; Helmi et al. 2018), also hampering the detection of low-mass mergers. Similarly, the population of clusters in the Galactic halo is mostly homogeneous in their [α/Fe] abundances (Recio-Blanco 2018).

* Full Table 2 is only available at the CDS via anonymous ftp to cdsarc.u-strasbg.fr (130.79.128.5) or via http://cdsarc.u-strasbg.fr/viz-bin/cat/J/A+A/648/A108

Table 1. Adopted references for yttrium, europium, and magnesium abundances.

Population	[Y/Fe] and [Eu/Fe] references	[Mg/Fe] references
Milky Way clusters	Johnson et al. (2017) and references in their Table 5, McWilliam et al. (1992), Shetrone et al. (2003), Muñoz et al. (2013), Roederer & Sneden (2011), Massari et al. (2017), James et al. (2004)	Recio-Blanco (2018)
Milky Way field stars	Fishlock et al. (2017), Roederer et al. (2014)	Nissen & Schuster (2010) Abolfathi et al. (2018)
Satellite field stars	Suda et al. (2008)	Suda et al. (2008)

Galactic archaeology thus needs a new accretion diagnostic to understand the primordial stellar populations and, in this work, we used neutron-capture elements to identify this diagnostic. Contrary to α-elements, neutron-capture elements present unexplained large abundance spreads for low-metallicity stars, which could result from a mixture of formation sites. In particular, we considered the logarithm of the ratio of the yttrium abundance of a star with respect to its europium abundance, [Y/Eu]. Approximately 75% of the solar yttrium was produced (Prantzos et al. 2018) by low- and intermediate-mass asymptotic giant branch (AGB) stars, through slow neutron captures (relative to the β-decay rates of unstable nuclei). In addition, first peak s-elements such as Y have a larger contribution from low-mass stars than second peak elements such as Ba. On the other hand, 94% of europium is produced by massive stars through rapid neutron captures (Bisterzo et al. 2014). Proposed Eu production sites are neutron star mergers (Rosswog et al. 1999), high-energy winds accompanying core collapse supernovae explosions (Woosley et al. 1994), or magneto-hydrodynamical explosions of fast-rotating stars (Winteler et al. 2012). As a consequence, the [Y/Eu] abundance ratio characterizes the relative contribution of low- to intermediate-mass stars with respect to high-mass stars, which is therefore a good indicator of the chemical evolution efficiency.

2. Chemical abundances database

The present study relies on several samples of objects: globular clusters and field stars, both from the Milky Way and its satellites. We made use of abundances of europium, yttrium, and [Mg/Fe], collected from multiple literature works. The adopted references for the abundances of the different elements and populations analysed in this work are summarized in Table 1.

The analysed Milky Way field stars abundances come from three different compilations: a photometric selection of metal-poor stars (Roederer et al. 2014), a study of heavy-element abundances for high-α and low-α stars at intermediate metallicity (Fishlock et al. 2017), and a selection of high transversal velocity stars from the Apache Point Observatory Galactic Evolution Experiment (APOGEE) survey (Abolfathi et al. 2018). When considering the field star homogeneous abundances from Roederer et al. (2014), we only take into account stars with abundances estimated from three or more lines to select a high-quality sample. We do not consider stars for which only upper limits were provided. The APOGEE sample is composed of *Gaia* DR2 stars with parallax >0.3 mas, $G < 15$ mag and Vtot > 180 km s^{-1}. Our final sample comprises 972 objects with APOGEE DR14 [Mg/Fe] abundances. The study of globular clusters chemical abundances is currently confined to heterogeneous compilations from different groups (see Table 1). Nevertheless, despite these words of caution, clusters benefit today from several decades of effort in chemical abundance estimations. The complete sample of 1033 Milky Way objects is reduced to 53 objects with good quality estimates of Fe, Y, Eu, and Mg. This Milky Way control group allows us to directly study the correlation between heavy elements and α-elements in our Galaxy (cf. Sect. 5).

In addition, the chemical abundances of Milky Way satellites were analysed using a compilation with metallicities [Fe/H] < −0.5 dex, obtained from the SAGA database (Suda et al. 2008). We gather stars with Y, Eu, and Mg abundance determinations, excluding those with only upper limits, carbon-enriched stars (defined as [C/Fe] < 0.9 dex if [Fe/H] < −1.0 dex), and objects reported as binaries. The total sample comprises 115 stars in satellites, with estimates of Fe, Mg, Y, and Eu.

Concerning the [Y/Eu] uncertainty estimates, we examined the abundance dispersion of the objects analysed by more than one study, including the dwarf stars database. The mean dispersion in the [Y/Eu] ratio is 0.07 dex, indicating a reasonable agreement between multiple literature sources. To adopt a conservative value, we multiplied that dispersion by 2, adopting a typical error bar of 0.15 dex. Moreover, it is worth noting that, apart from the objects analysed by Fishlock et al. (2017) and Nissen & Schuster (2010) in the metal-rich regime, the targets considered in this work are all giants or sub-giants, limiting potential biases due to gravity trends. Concerning NLTE corrections, Mashonkina et al. (2012) reported positive corrections ranging from 0.05 to 0.10 dex, with mean differences of about 0.03 dex between dwarfs and giants (larger corrections for lower gravities are estimated). These differences are therefore within the adopted error bars in this work. Finally, we found five stars in common between the APOGEE and the Nissen & Schuster (2010) samples. The mean difference in the [Mg/Fe] abundances is 0.02 ± 0.02 dex, again within the adopted errors. The complete set of abundances used in this work is included in the electronic version of Table 2.

3. Orbital parameter estimations

We complemented the chemical analysis of Milky Way objects with orbital parameters based on *Gaia* data (Gaia Collaboration 2018a). For globular clusters, the orbital parameters were taken from Model-2 in Gaia Collaboration (2018b). These orbital parameters were computed as the average values over 10 Gyr of integration. To this purpose, we used the median values obtained from 1000 orbits for each cluster obtained through Monte Carlo realizations of the initial conditions, considering the observational measurements and their errors. In particular, the average inclination of an orbit was computed as arccos (Lz/Ltot). In our convention, the orbital inclination is defined from the Galactic plane and comprised between 0° and 180°, with prograde orbits below 90°. Error bars in the orbital parameters associated with model assumptions were estimated by comparing the results

Table 2. Sample of chemical abundances and orbital parameters used in this work.

Reference	ID	[Fe/H] (dex)	[Mg/Fe] (dex)	[Y/Fe] (dex)	[Eu/Fe] (dex)	Orbital inclination (degrees)
Roederer et al. (2014)	CS 22957-013	−2.98	0.47	−0.80	−0.27	139
Roederer et al. (2014)	CS 22960-064	−2.77	0.44	−0.18	0.35	28
Roederer et al. (2014)	CS 29513-014	−2.32	0.45	0.08	0.24	53
...	...	...	...	...	...	...

Notes. The complete version of the table is available at the CDS.

obtained with different Galactic potentials (defined as Model-1, -2, -3 in Gaia Collaboration 2018b). In particular, the dispersion in the orbital inclination (estimated as the third quantile value of the differences distribution between two models) is six degrees. In addition to this main dataset of cluster orbits, we completed the sample with six additional objects from Vasiliev (2019).

For our field stars samples, we derived the orbital parameters using the Python package galpy (Bovy 2015). We assume the MWPotential14 Milky Way mass model included in this package. We derived the action parameters through the action-angle isochrone approximation (Bovy 2014). As input parameters we used the radial velocities gathered in Simbad, the *Gaia* DR2 proper motions, and the distances from Bailer-Jones et al. (2018). In addition, we checked the effect of using two different methodologies of the dynamical parameters for clusters and field stars. To this purpose, we re-computed the clusters orbital inclinations using the field stars methodology calculated the differences with respect to the Model-2 orbital results from Gaia Collaboration (2018a,b). The median absolute deviation of the orbital inclination differences is 2.5 degrees, confirming the consistency of the two approaches.

Finally, we assessed the impact of the detected *Gaia* kinematic biases (Schönrich et al. 2019) in our data. For the field star samples, only 18 targets had a few parameters outside the Schoenrich et al. quality cuts and were excluded from the analysis. Regarding the globular cluster data, the Gaia Collaboration (2018b) database is within the quality cuts, and the Vasiliev et al. compilation uses literature distances and line-of-sight velocities not concerned by the *Gaia* parallax bias. The complete set of orbital inclinations used in this work is included in the electronic version of Table 2.

4. [Y/Eu] and [Mg/Fe] abundance ratios in dwarf galaxies of different luminosities

First of all, we analysed the [Y/Eu] behaviour with respect to the [Mg/Fe] turnovers for satellite galaxies of different masses. Figure 1 shows the Mg abundance (an α-element) with respect to iron as a function of [Fe/H] for stars belonging to the low-mass satellites Ursa Minor, Draco, and Carina and to the higher-mass satellites Fornax, Sculptor, and Leo I. The points are colour coded by the stars [Y/Eu] content. It can be observed that higher-luminosity systems, for which the [Mg/Fe] abundance declines at higher metallicities, present enhanced [Y/Eu] abundances, particularly in the [Fe/H] regime between −2.25 dex and −1.25 dex.

To better understand the [Y/Eu] behaviour, a separate study of [Eu/Fe] and [Y/Fe] abundance trends with [Mg/Fe], for Milky Way satellites of different luminosities, was performed. Figure 2 shows again the same objects and [Mg/Fe] abundances of Fig. 1 using a colour code on the [Eu/Fe] and [Y/Fe] abundances for panels a and b, respectively. Stars showing high [Mg/Fe] values present lower [Eu/Fe] abundances than those of similar metallicity with lower [Mg/Fe] values. As a consequence, stars with [Eu/Fe] abundances lower than about 0.5 dex display low [Mg/Fe] abundances only for metallicities higher than around −1.75 dex, suggesting a faster chemical evolution of their parent systems. Conversely, at a given metallicity, higher [Mg/Fe] stars tend to have similar [Y/Fe] values as lower [Mg/Fe] stars. This suggests that lower-mass systems tend to present higher [Eu/Fe] enrichments and similar [Y/Fe] abundances than more massive systems, in their overlapping metallicity range below −1.25 dex, conducting to higher [Y/Eu] ratios as shown in Fig. 1.

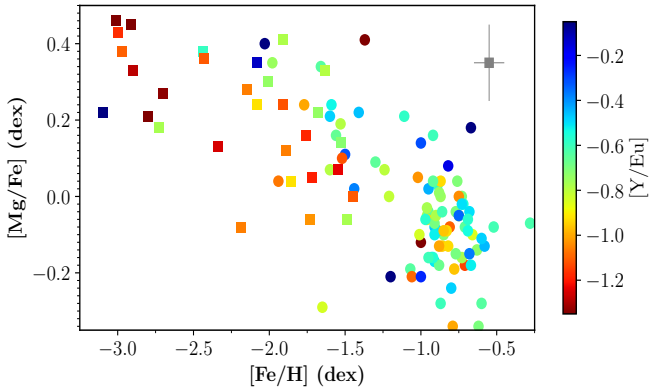

Fig. 1. Mg abundance with respect to iron as a function of [Fe/H] for stars belonging to low-mass satellites (Ursa Minor, Draco, and Carina; square symbols) and to higher-mass satellites (Fornax, Sculptor, and Leo I; circles). The points are colour coded by the stars [Y/Eu] content.

Moreover, to quantify the homogeneity of the different abundance ratios across all [Fe/H], Fig. 3 shows the abundance histograms of [Y/Eu], [Mg/Fe], [Y/Fe], and [Eu/Fe] in three different metallicity intervals, from the metal-poor regime on the left, to the metal-rich regime on the right. The mean abundance values and their dispersion are indicated on each panel. First of all, only the [Y/Eu] and the [Mg/Fe] mean ratios show a clear metallicity dependence. On one hand, the [Y/Eu] mean abundance is lower in the metal-poor regime in which low-mass satellites dominate, increasing progressively with metallicity, reaching the highest value in the metal-rich regime in which higher-mass satellites prevail. On the other hand, the [Mg/Fe] mean value shows the expected behaviour of an [α/Fe] diagnostic, decreasing with metallicity. The other two abundance ratios, [Y/Fe] and [Eu/Fe], do not present clear metallicy trends through the entire [Fe/H] range, possibly as a consequence of the different nucleosynthetic channels at play. For both [Y/Fe] and [Eu/Fe], the higher mean value is found in the metal-poor regime, where the r-process nucleosynthesis also dominates for yttrium. In addition, Eu is clearly over-abundant with respect Y at low metallicities, leading to the lowest [Y/Eu] mean value observed. In the metal-intermediate regime, both the [Y/Fe] and the

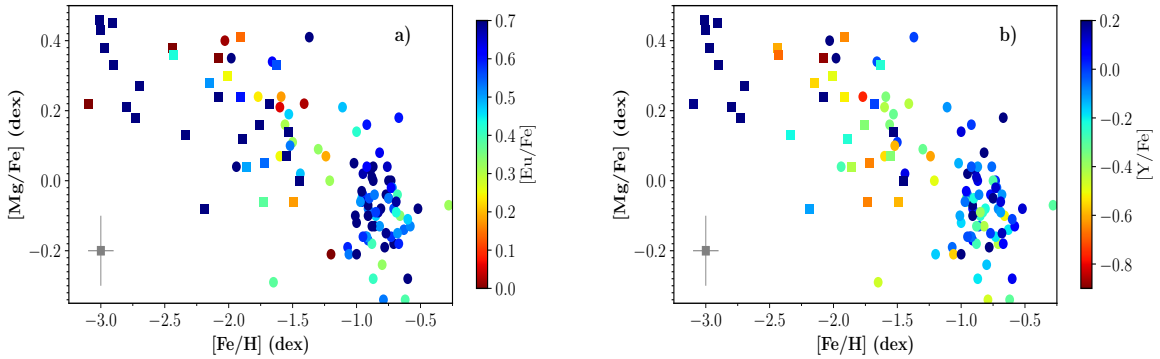

Fig. 2. Mg abundance with respect to iron as a function of [Fe/H] for stars belonging to low-mass satellites (Ursa Minor, Draco, and Carina; square symbols) and to higher-mass satellites (Fornax, Sculptor, and Leo I; circles). The points are colour coded by the stars [Eu/Fe] content (*panel a*) and by their [Y/Fe] abundance (*panel b*).

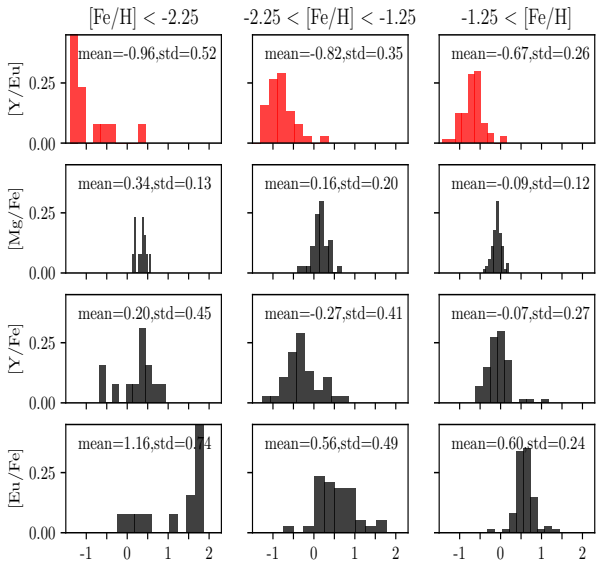

Fig. 3. Mg abundance with respect to iron as a function of [Fe/H] for stars belonging to low-mass satellites (Ursa Minor, Draco, and Carina; square symbols) and to higher-mass satellites (Fornax, Sculptor, and Leo I; circles). The points are colour coded by the stars [Y/Eu] content.

[Eu/Fe] mean values decrease, possibly owing to the arrival of the type Ia SN Fe contribution. Finally, while the [Eu/Fe] ratio continues to decrease, the [Y/Fe] rises again in the metal-rich regime, after the onset of the s-process contribution to yttrium. The combination of the Y under-abundance with respect to Eu in the metal-poor domain, and the progressive arrival of the s-process yttrium contribution as metallicity increases, leads to a constant increasing trend of the [Y/Eu] mean values with metallicity.

5. Chemo-dynamical correlations and abundance spread in the halo

Following the results in the previous section, the observed [Y/Eu] abundance spread in our Milky Way could result from a mixture of systems with different masses. If this is the case, the [Y/Eu] indicator should be compatible with the commonly used [Mg/Fe] accretion diagnostic in our Galaxy as well. This has already been observed in the high-metallicity regime (Fishlock et al. 2017), but it is difficult to test in the metal-poor regime, where the [α/Fe] spread is very low.

Figure 4 shows the control group of 53 Milky Way objects with available Fe, Mg, Y, and Eu abundances. As shown in the left panel, the objects span the entire metallicity range and include both high [Mg/Fe] and low [Mg/Fe] objects. The right panel illustrates the [Mg/Fe] abundances as a function of [Y/Eu], putting the two diagnostics against each other, for Milky Way objects. A mild correlation is observed at all metallicities. However, as a consequence of the saturation of the [Mg/Fe] diagnostic in the metal-poor regime, the trend is less significative for metal-intermediate and metal-poor objects.

Fortunately, since the arrival of precise *Gaia* astrometric data, dynamical information can be used to break down this degeneracy. Chemo-dynamical correlations retrieved both in the [Mg/Fe] and the [Y/Eu] spread could reinforce the [Y/Eu] abundance as a good accretion indicator. To test this possibility, we classified our Milky Way objects into three categories, using the [Y/Eu] and the [Mg/Fe] criteria independently (upper and lower panels of Fig. 5, respectively). First, objects with depleted [Y/Eu] values or metal-poor [Mg/Fe] turnovers (red targets) compatible with low-mass progenitors; second, objects with intermediate [Y/Eu] abundances or intermediate-metallicity [Mg/Fe] turnovers (green targets) possibly formed in higher-mass systems; and third, targets with enhanced [Y/Eu] values or a metal-rich [Mg/Fe] turnover typical of the Milky Way in situ population (blue objects). The standard value used for the [Y/Eu] separation (black line in Fig. 5) was defined by a theil-sen linear fit of the data. The [Mg/Fe] selected samples act here as validation groups testing the [Y/Eu] diagnostic independently.

Panels c and d show the normalized distribution of orbital inclinations for the three sets of objects, selected either with the [Y/Eu] diagnostic or with the [Mg/Fe] diagnostic, respectively. Although the two chemical diagnostics target different objects (those in common being excluded from panel d histograms) and span different metallicity regimes, the similarities between panels c and d distributions are important. Two-sampled Kolmogorov-Smirnov tests between the nine possible pairs of distributions were performed to test this similarity. The null hypothesis, assuming that the samples come from a population with the same distribution, is rejected for all the pairs except those of the same colour (targeting therefore the same parent system mass). In particular, depleted [Y/Eu] objects tend to present high orbital inclinations, as targets with a metal-poor [Mg/Fe] turnover. On the contrary, objects with intermediate [Y/Eu] abundances and intermediate metallicity [Mg/Fe] turnovers display mainly low-inclination retrograde orbits. Finally, targets with high [Y/Eu] ratios and metal-rich [Mg/Fe] turnovers primarily show low-inclination prograde orbits. As expected, adjacent

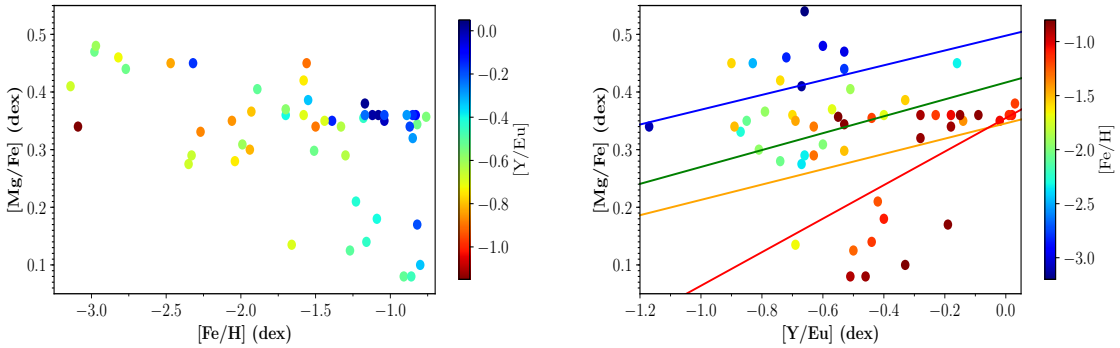

Fig. 4. Control group of Milky Way objects with available Fe, Mg, Y, and Eu abundances. *Left panel*: Mg abundance with respect to iron as a function of [Fe/H] for the Milky Way sample stars with available estimates of [Y/Eu] abundance (included in the colour bar). *Right panel*: [Mg/Fe] as a function of [Y/Eu] the same Milky Way control group, colour coded by the [Fe/H] abundance. The linear correlations between [Mg/Fe] and [Y/Eu] in four metallicity intervals (less than [Fe/H] = −2.1 dex, between −2.1 dex and −1.5 dex, between −1.5 dex and −1.1 dex, and above [Fe/H] = −1.1 dex) are included as solid lines, following the [Fe/H] abundance colour code.

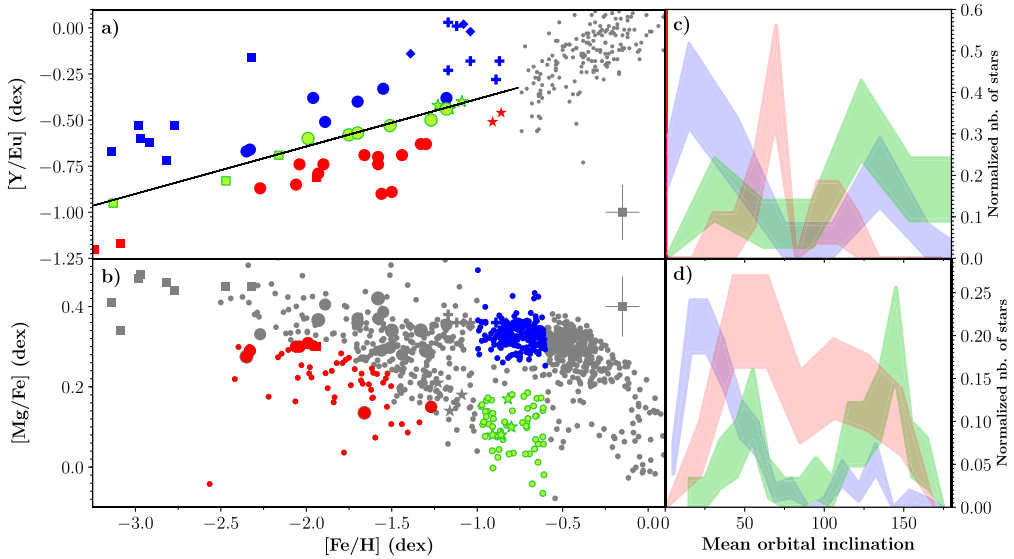

Fig. 5. Analysis of correlations between chemical abundances and orbital inclination. *Panel a*: yttrium abundance with respect to europium as a function of iron abundance for Milky Way globular clusters (large circles) and field stars (squares for a metal-poor sample (Roederer et al. 2014), diamonds, stars, and crosses for an intermediate-metallicity compilation (Fishlock et al. 2017) of high [Mg/Fe], low [Mg/Fe] and thick disc stars, respectively). The colour code is based on the [Y/Eu] departures from the standard value (black line). *Panel b*: [Mg/Fe] abundance ratio with respect to iron for the previous objects, when available, and a compilation of high transversal velocity stars from APOGEE. The colour code selects groups with different [Mg/Fe] turnovers (thus parent system masses). *Panels c , d*: distributions of orbital inclinations for the groups selected with the [Y/Eu] and [Mg/Fe] criteria, respectively.

groups in [Y/Eu] or [Mg/Fe] abundances (red-green and green-blue pairs), partially overlap in their orbital inclination distributions as a result of abundance uncertainties, but also because no perfectly separated components seem to exist. In particular, in situ formed objects dynamically heated by past mergers (e.g., Belokurov et al. 2019; Di Matteo et al. 2019) could also blur the orbital inclination distributions.

The above result confirms the coherence of the [Y/Eu] diagnostic with the [Mg/Fe] diagnostic, revealing possible chemo-dynamical correlations with two independent chemical indicators. To quantify those trends, Fig. 6 shows the deviations in [Y/Eu] and [Mg/Fe] abundances with respect to the average, as a function of orbital inclination. Contrary to the analysis of Fig. 5, no data subsamples are predefined. Again, the average values are defined through a theil-sen linear fit of the data, being 0.258·[Y/Eu] − 0.16 and −0.12·[Mg/Fe] + 0.13, in the upper and lower panels of Fig. 6, respectively. The two chemical diagnostics show under-abundances around the polar direction (60° $\lesssim$ inclination $\lesssim$ 120°) and over-abundances near to the plane (prograde objects with inclination $\lesssim$ 60° and retrograde objects with inclination $\gtrsim$120°). The observed chemo-dynamical correlations, including both globular clusters and field stars, are more pronounced for the [Y/Eu] abundances than for the [Mg/Fe] abundances as expected from their corresponding abundance spreads in this metallicity regime. In particular, the orbital inclination seems to account for about half of the [Y/Eu] abundance scatter.

6. Conclusions

Although Galactic studies constantly need to be validated in the huge parameter space of Milky Way populations, the observed chemo-dynamical correlations open new paths of exploration of our Galaxy formation history. In the light of previous conclusions, the heavy elements abundance scatter of the primordial Milky Way possibly results from an amalgam of systems with different masses and chemical evolutions.

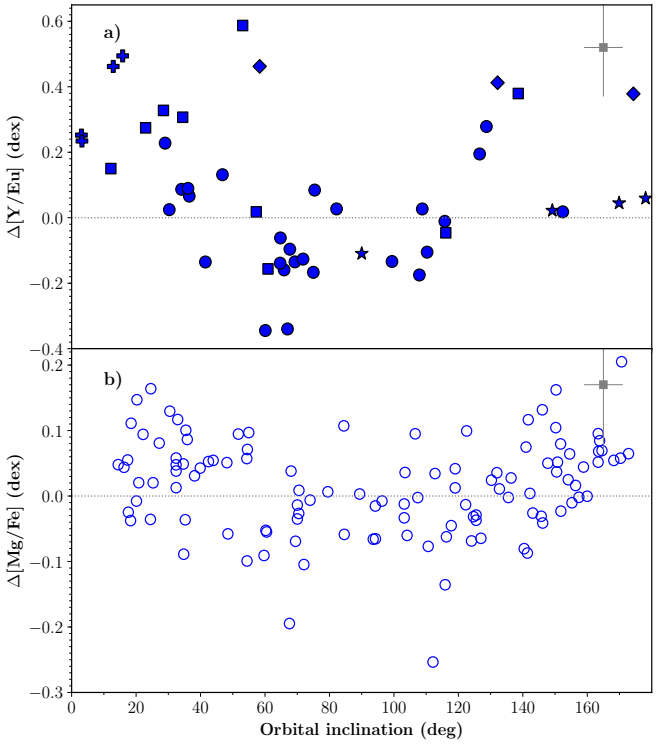

Fig. 6. Deviations in [Y/Eu] (*panel a*) and [Mg/Fe] (*panel b*) abundances, with respect to the average, as a function of the orbital inclination. No objects in common to the [Y/Eu] and the [Mg/Fe] analysis are included. Average values were defined by a Theil-Sen linear fit for each abundance trend with metallicity.

First, objects in polar-like orbits showing under-abundances of [Y/Eu] could result from a composite debris from low-mass accretions. Interestingly, polar orbits are also found for more recent merger events as the Sagittarius event. This suggests the possible existence of a preferential accretion axis around the polar direction, linking the Milky Way to its satellites and deserving further study. In the metal-poor and intermediate-metallicity regime, where the [Y/Eu] under-abundances are larger than [α/Fe] under-abundances, future large-scale, heavy-element studies seem crucial to distinguish between low-mass accretions and slow-rotating debris from more massive mergers.

Second, satellite merger debris in retrograde orbits was previously suggested by the analysis of several dynamical over-densities (e.g., Helmi et al. 2018; Belokurov et al. 2018; Myeong et al. 2019) and attributed to high-mass progenitors (*Gaia* Enceladus/Saussage, Sequoia). In our study, the chemical patterns dominating that retrograde regime near to the plane are typical of high-mass systems, reaching metallicities of −0.5 dex and relatively high [Y/Eu] abundances. The interplay of this old retrograde population with the prograde disc and the slow-rotating accretion debris is probably an important piece of the Galaxy formation puzzle.

Third, a prograde population, showing [Y/Eu] over-abundances, seems to be present even in the low-metallicity regime. It could be the fossil signature of the primitive collapsed Galaxy, probably occupying prograde orbits near to the plane, as the more metal-rich disc. This hypothesis is strengthen by the recent discovery of very metal-poor stars with disc-like orbits (Sestito et al. 2020)

In conclusion, both nature and nurture appear to have played a role to build up the ancient Milky Way, leaving imprints we are starting to decode. The present conclusions will be strengthened by a future analysis including more r-process and s-process elements (Fernández-Alvar et al., in prep.). Chemical diagnostics, including heavy elements abundances, will certainly be fundamental in the ongoing *Gaia* revolution.

Acknowledgements. This work has made use of data from the European Space Agency (ESA) mission *Gaia* Data Processing and Analysis Consortium (https://www.cosmos.esa.int/gaia), processed by the *Gaia* Data Processing and Analysis Consortium. (DPAC, https://www.cosmos.esa.int/web/gaia/dpac/consortium). Funding for the DPAC has been provided by national institutions, in particular the institutions participating in the *Gaia* Multilateral Agreement. ARB, PdL and EFA acknowledge financial support from the ANR 14-CE33-014-01. TA has received funding from the European Union's Horizon 2020 research and innovation programme under Marie Sklodowska-Curie grant agreement number 745617 and also acknowledges funding from the MINECO (Spanish Ministry of Economy) through grants ESP2016-80079-C2-1-R (MINECO/FEDER, UE) and ESP2014-55996-C2-1-R (MINECO/FEDER, UE). AH acknowledges funding from a Vici grant from the Netherlands Organisation for Scientific Research (NWO). We thank E. Vasiliev for providing his orbital parameters for globular clusters. ARB thanks Vanessa Hill, Sebastian Peirani and Oliver Hahn for useful discussions and Chris Wegg for language corrections.

References

Abolfathi, B., Aguado, D. S., Aguilar, G., et al. 2018, ApJS, 235, 42
Bailer-Jones, C. A. L., Rybizki, J., Fouesneau, M., Mantelet, G., & Andrae, R. 2018, AJ, 156, 58
Belokurov, V., Erkal, D., Evans, N. W., Koposov, S. E., & Deason, A. J. 2018, MNRAS, 478, 611
Belokurov, V., Deason, A. J., Erkal, D., et al. 2019, MNRAS, 488, L47
Belokurov, V., Sanders, J. L., Fattahi, A., et al. 2020, MNRAS, 494, 3880
Bisterzo, S., Travaglio, C., Gallino, R., Wiescher, M., & Käppeler, F. 2014, ApJ, 787, 10
Bovy, J. 2014, galpy: Galactic Dynamics Package
Bovy, J. 2015, ApJS, 216, 29
Di Matteo, P., Haywood, M., Lehnert, M. D., et al. 2019, A&A, 632, A4
Fishlock, C. K., Yong, D., Karakas, A. I., et al. 2017, MNRAS, 466, 4672
Freeman, K., & Bland-Hawthorn, J. 2002, ARA&A, 40, 487
Gaia Collaboration (Brown, A. G. A., et al.) 2018a, A&A, 616, A1
Gaia Collaboration (Helmi, A., et al.) 2018b, A&A, 616, A12
Helmi, A., Babusiaux, C., Koppelman, H. H., et al. 2018, Nature, 563, 85
James, G., François, P., Bonifacio, P., et al. 2004, A&A, 414, 1071
Jean-Baptiste, I., Di Matteo, P., Haywood, M., et al. 2017, A&A, 604, A106
Johnson, C. I., Caldwell, N., Rich, R. M., et al. 2017, ApJ, 842, 24
Koppelman, H. H., Bos, R. O. Y., & Helmi, A. 2020, A&A, 642, L18
Mashonkina, L., Ryabtsev, A., & Frebel, A. 2012, A&A, 540, A98
Massari, D., Mucciarelli, A., Dalessandro, E., et al. 2017, MNRAS, 468, 1249
Matteucci, F., & Greggio, L. 1986, A&A, 154, 279
McWilliam, A., Geisler, D., & Rich, R. M. 1992, PASP, 104, 1193
Muñoz, C., Geisler, D., & Villanova, S. 2013, MNRAS, 433, 2006
Myeong, G. C., Vasiliev, E., Iorio, G., Evans, N. W., & Belokurov, V. 2019, MNRAS, 488, 1235
Nissen, P. E., & Schuster, W. J. 2010, A&A, 511, L10
Prantzos, N., Abia, C., Limongi, M., Chieffi, A., & Cristallo, S. 2018, MNRAS, 476, 3432
Ratcliffe, B. L., Ness, M. K., Johnston, K. V., & Sen, B. 2020, ApJ, 900, 165
Recio-Blanco, A. 2018, A&A, 620, A194
Roederer, I. U., & Sneden, C. 2011, AJ, 142, 22
Roederer, I. U., Preston, G. W., Thompson, I. B., et al. 2014, AJ, 147, 136
Rosswog, S., Liebendörfer, M., Thielemann, F. K., et al. 1999, A&A, 341, 499
Schönrich, R., McMillan, P., & Eyer, L. 2019, MNRAS, 487, 3568
Sestito, F., Martin, N. F., Starkenburg, E., et al. 2020, MNRAS, 497, L7
Shetrone, M., Venn, K. A., Tolstoy, E., et al. 2003, AJ, 125, 684
Suda, T., Katsuta, Y., Yamada, S., et al. 2008, PASJ, 60, 1159
Suda, T., Hidaka, J., Aoki, W., et al. 2017, PASJ, 69, 76
Tinsley, B. M. 1979, ApJ, 229, 1046
Vasiliev, E. 2019, MNRAS, 484, 2832
Winteler, C., Käppeli, R., Perego, A., et al. 2012, ApJ, 750, L22
Woosley, S. E., Wilson, J. R., Mathews, G. J., Hoffman, R. D., & Meyer, B. S. 1994, ApJ, 433, 229